Advance Publication Cover Page

Chemistry Letters

Highly Catalytically Active High-spin Single-Atom Iron Catalyst Supported by Catechol-Containing Microporous 2D Polymer

Guangwen Li, Defa Gu, Rui Cao, Song Hong, Yushan Liu, and Yuzhou Liu*

Advance Publication on the web July 23, 2020
doi:10.1246/cl.200416

Highly Catalytically Active High-spin Single-Atom Iron Catalyst Supported by Catechol-Containing Microporous 2D Polymer

Guangwen Li[1,#], Defa Gu[1,#], Rui Cao[2], Song Hong[3], Yushan Liu[4], Yuzhou Liu[1,5*]

1 School of Chemistry, Beihang University, Beijing 100191, China

2 Stanford Synchrotron Radiation Lightsource, SLAC National Accelerator Laboratory, Menlo Park, California 94025, United States

3 Center for Instrumental Analysis, Beijing University of Chemical Technology, Chaoyang, Beijing 100029, China

4 Trinity school of Durham and chapel Hill, Durham and chapel Hill, Durham, NC, 27708, USA

5 Beijing Advanced Innovation Center for Biomedical Engineering, Beihang University, Beijing 100191, China

# G.L. andD.G. contributed equally.

E-mail: liuyuzhou@buaa.edu.cn

Traditionally, Fe-SACs are prepared through energy-intense processes, which often lead to the loss of precision in structural features from the starting substrates and impeding rational design. We herein described the synthesis of a unique catechol-containing porous polymer with designed features in the substrates maintained, affording atomically dispersed iron catalyst (Fe-SAC) through treatment of ferrous chloride ($FeCl_2$). An aberration-corrected scanning transmission electron microscope (AC-STEM) and synchrotron X-ray absorption spectroscopy (XAS) were employed to shed light on the local coordination geometry of the atomically dispersed iron catalyst. The resulting Fe-SAC exhibits excellent catalytic performance in reduction of nitroaromatics with highest molar K_{app} among all Fe based catalysts.

Keywords: porous organic polymer, catechol, single-atom iron catalyst

Supported transition metal complexes represent the majority of catalysts used in heterogeneous catalysis, and one main research goal in this area is minimizing the size of transition metal nano particles aximize the loading of active sites and catalytic efficiency. Recent emergence of single-atom catalysts (SACs) has offered additional incentives due to new opportunities associated with this possibly smallest size [1]. Early examples of the supported SACs mostly involved nobel transition metal elements, such as platinum (Pt) [2], palladium (Pd) [3], ruthenium (Ru) [4], and gold (Au) [5], while efficient catalytic activities have been reported employing these noble metal catalysts, their low earth's crust abundance has prompted the development of SACs based on other widely available elements. Iron (Fe) is the most abundant transition metal element, and the preparation of highly active iron-based SACs (Fe-SACs) are undoubtedly attractive, especially considering recent reports about their higher activity than Pt catalysts in oxygen reduction reaction [6].

Currently iron SACs (Fe-SACs) are mainly prepared through energy-intense processes such as carbonization [7], [8] and ball-milling[9]. One inevitable problem with these harsh processes is that the original structures are always damaged to some degree and the exact structural parameters of the resulting materials are uncontrollable. The lack of full appreciation and control of the structural features of Fe-SACs thus has hampered the efforts trying to elucidate the correlation between structures and catalytic performance. Incorporation of this structurally well-defined model into Fe-SAC research can greatly speed up the development of new and potent Fe-SACs, but the prerequisite is the development of a benign preparation process, which has remained elusive with scarce and isolated examples [10].

Different from noble metal complexes, iron catalysts can benefit from spin state manipulation, and the high-spin state iron catalysts are of special interest due to their high catalytic activity in many reactions [11, 12, 13]. In fact, natural enzymes such as intradiol dioxygenases also possess high spin state iron as the catalytically active centers[14]. Incorporation of high spin iron centers in SACs in a controllable manner is therefore of significant importance. Although high spin-state Fe-SACs have been previously reported [15], these are actually "after-the-fact" results, and there is no clear and reliable design principle to follow due to the harsh preparing conditions. How to purposefully design a high-spin Fe-SAC has remained unknown.

Herein, we report a rational design and preparation of high-spin Fe SAC with benign synthesis condition through the use of catechol groups. Our design has been based on the following rationales. First, the iron-catechol bond with covalent nature [16] has been one of the strongest interactions, commonly utilized in material science [17] and biological siderophores [18], and can therefore facilitate iron attachment without harsh treatment. Second, the iron/catechol bond has been demonstrated as high spin [19], and therefore a high spin Fe-SAC is expected with catechol as the anchoring groups. Third, the plantation of catechol in a rigid porous polymer can prevent saturated coordination and leave unsaturated coordination sites for catalysis.

Following these concepts, a catechol-containing microporous polymer with graphitic units has been synthesized, and then the fabrication of the Fe-SAC is performed with ethanolic $FeCl_2$ treatment and subsequent heating at 100 ^{o}C through the strong catechol-iron interaction. The Fe-SAC is characterized by various methods including an aberration-corrected scanning transmission electron microscope (AC-STEM) and synchrotron X-ray absorption spectroscopy (XAS), confirming the single-atom distribution and high spin-state of supported Fe atoms. The benign synthesis condition allows transferring of the structural information of the precursors onto the SAC, enabling a successful design in the way that graphitic catechol units lead to expected generation of a high-spin Fe-SAC. Other structural features such as the

curvature and bulkiness of the precursors are also maintained, thwarting the inter-layer stacking and promoting maximum dispersion of the Fe-SAC. The dispersible high spin Fe SAC exhibits the highest catalytic activity among all heterogeneous iron-based catalysts hitherto in 4-nitrophenol reduction by $NaBH_4$ up to now.

The synthesis of our catechol containing porous polymer is inspired by a previously reported method for the synthesis of a series of graphitic organic molecules, in which 1,3,5-tribenzylbenzene (compound **1**) reacts with mono-aldehyde in one-pot to form various hexabenzocoronene derivatives with high yields [20]. We reason that the use of di-aldehyde fluorene (compound **2**) will lead to the generation of a two-dimensional porous graphene polymer (**POG-OMe**), and subsequent hydrolysis of the methoxy groups can release the catechol groups to generate the anticipated polymer (**POG-OH**). As shown in Fig. 1a, the reaction between compound **1** and **2** smoothly affords the anticipated conjugated 2D polymers **POG-OMe** after oxidation with excessive $FeCl_3$. Deconvoluted C1s XPS peaks in Fig. S8a show the characteristic conjugated sp^2 carbon (284.7 eV), and the peaks at 285.5 and 286.5 eV are assigned to sp^3 carbon atoms of C-C and C-O bonds respectively [21]. The O1s XPS spectrum in Fig. S8b at 533.2 eV is due to the O-C bonds, consistent with C1s spectrum analysis [22]. As shown in Fig. S8c, Raman spectroscopy confirms the existence of graphitic carbon at 1590 cm^{-1} and 1350 cm^{-1}, which are expected for the conjugated graphitic macromolecules [23]. The porosity of **POG-OMe** is investigated with N_2 adsorption-desorption experiments at 77 K. As shown in Fig. 1b, it displays a rapid uptake at low relative pressures ($P/P_0 < 0.001$), indicating the presence of substantial amount of micropores. NLDFT [24] calculation reveals that **POG-OMe** predominantly contains micropores of 1.67 nm in size (Fig. 1b), which is consistent with the calculated values of 1.68 nm based on a structural model of **POG-OMe** (Fig. S9). The BET surface area for **POG-OMe** is as large as 848 m^2 g^{-1}. In addition, **POG-OMe** is mainly amorphous according to its PXRD spectrum (Fig. S10), and this is also expected for porous polymers constructed with irreversible covalent bonds.

POG-OMe is treated with excessive BBr_3 and then water to provide **POG-OH** in a quantitative yield. As shown in Fig. 1c, the IR analysis clearly reveals the complete disappearance of C-O-C stretching vibration peak at 1112 cm^{-1} and emergence of a new peak at around 3500 cm^{-1} characteristic of O-H stretching, and therefore confirms the full hydrolysis of the methoxy groups into hydroxyl groups to generate catechol moieties. Solid state ^{13}C-NMR also provides evidences for the complete hydrolysis. The analysis of the ^{13}C-NMR spectra for **POG-OMe-S** and **POG-OH-S** (Fig. 1d, fully characterized by ^{1}H-NMR and MALDI-TOF, Figs. S4-7) shows the disappearance of the peaks at 55 ppm (C-O***C***H_3) and 150 ppm (***C***-OCH_3) and appearance of a new peak at around 142 ppm (***C***-OH) after hydrolysis. The similar spectrum changes between **POG-OMe** and **POG-OH** therefore supports the complete hydrolysis of all methoxy groups in **POG-OMe.**

With the presence of catechol groups, **POG-OH** is then used as the support for iron catalysts. 100 mg **POG-OH** is treated with iron (II) chloride solution in ethanol (8.9 mL, 1 mM, 0.03 eq. per catechol, 0.5 wt% Fe compared to **POG-OH**) at room temperature, and after filtration and washing by pure water, the sample is then heated at 100ºC for 24 hours to obtain **Fe@POG-OH** (see supporting information S2 for the details).

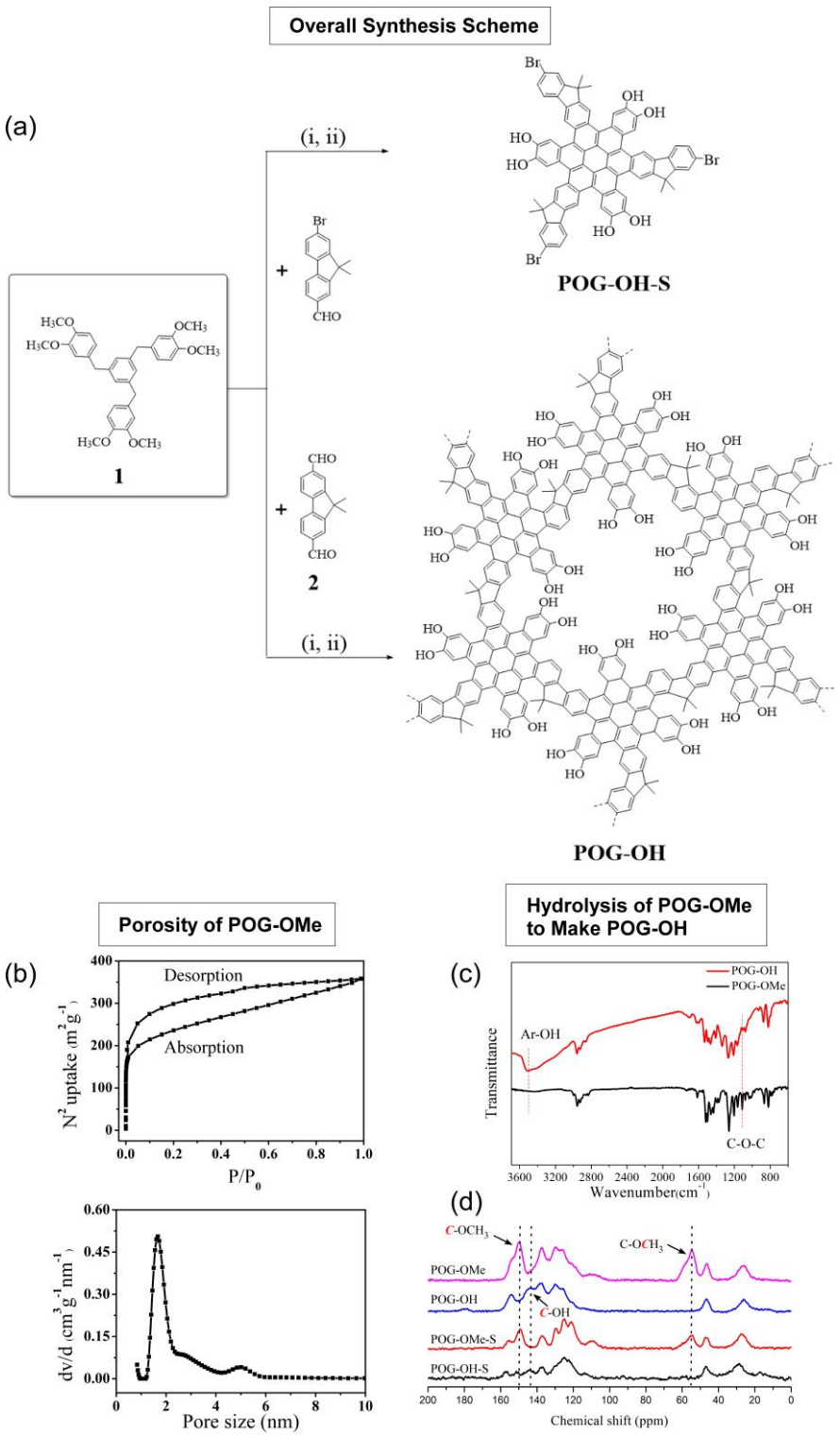

Figure 1. Overall synthesis scheme for **POG-OH**. (i) $FeCl_3$, Ac_2O, CH_2Cl_2, $MeNO_2$, rt (ii) CH_2Cl_2, BBr_3, 50 °C 48 h. **POG-OH-S** is a small monomer version of **POG-OH**. **POG-OMe-S** and **POG-OMe** stand for the relative hydrolysis precursors with methoxy groups. (**b-c)** Nitrogen adsorption-desorption isotherms and pore-size distribution of **POG-OMe**. (**d)** IR spectra of **POG-OMe** and **POG-OH**, showing the complete disappearance of C-O-C vibration and appearance of hydroxyl groups. (**e)** ^{13}C CP-MAS solid-state NMR spectra of **POG-OMe**, **POG-OH**, **POG-OMe-S** and **POG-OH-S**.

The structural details of **Fe@POG-OH** are revealed by atomic-resolution high-angle annular dark-field scanning transmission electron microscope (HAADF-STEM) analysis (Fig. 2). Isolated single Fe atoms are clearly identified as the bright dots around 0.1 nm. Energy dispersive X-ray spectroscopy (EDS) mapping confirm the uniform distribution of iron atoms on the support. It is estimated roughly 0.5 wt% iron has been loaded based on the EDS analysis (Fig. S11). Since initially 0.5 wt% Fe is used, the trapping efficiency is therefore almost quantitative.

The electronic structure and coordination geometry of the **Fe@POG-OH** are further interrogated via synchrotron X-ray absorption spectroscopy (XAS) (Fig. S14), In comparison with the Fe K-edge XANES spectrum of Fe foil (Fig. S15a, the yellow trace), a shift to a higher energy in the rising edge (between 7110 and 7125 eV) is observed for the **Fe@POG-OH** (Fig. 15a, the black trace), indicating the **Fe@POG-OH** is in a higher oxidation state and comparable with the edge shift found in Fe_2O_3 and $FeCl_3$ (Fig. S14a, the red and blue traces), where the Fe is known to possess the +3 oxidation state (ferric). XPS analysis (Fig. S12) confirms the high oxidation state of +3 for iron atoms [25]. The oxidation of original Fe (II) due to heating in air is common [26], and can explain detection of the Fe (III) in **Fe@POG-OH**.

The benign synthesis condition of **Fe@POG-OH** ensures that the structural information, such as symmetry, curvature and bulkiness, of **POG-OH** is intactly transferred to the final **Fe@POG-OH** to maintain porosity and dispersity.

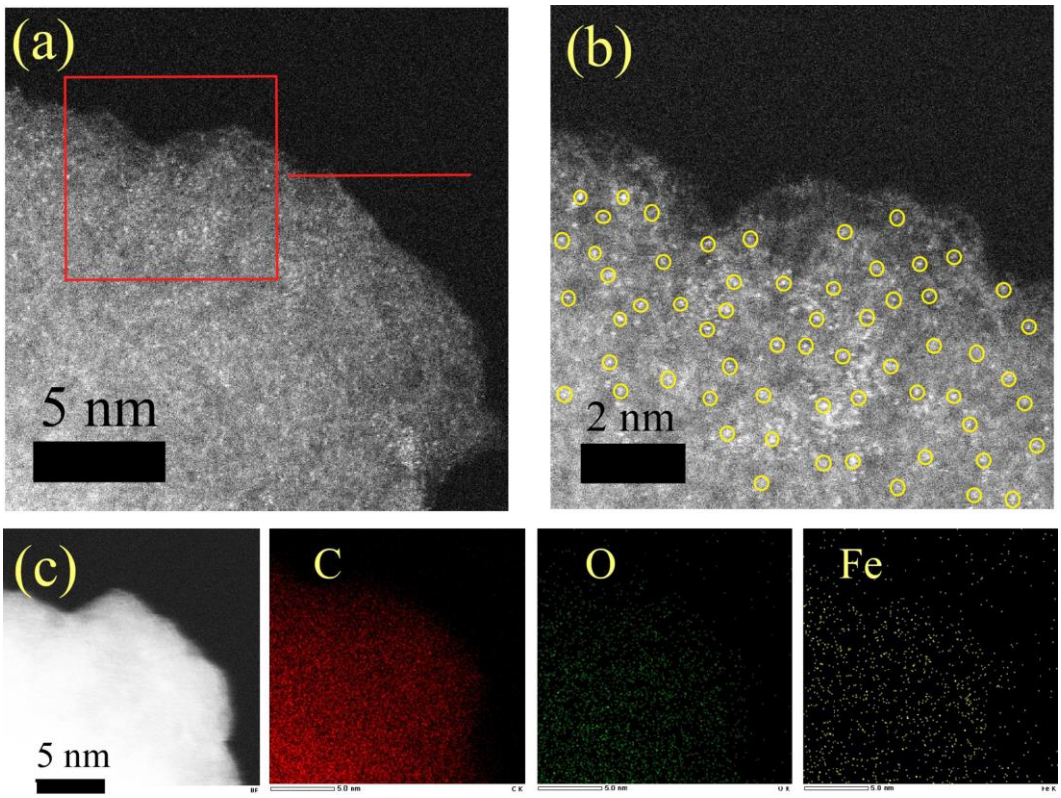

Figure 2. (a, b) HAADF-STEM images of **Fe@POG-OH** at different resolutions, (c) HAADF-STEM image and corresponding EDS elemental mapping (C, O and Fe) of **Fe@POG-OH**.

The benign synthesis condition also enables good dispersion of the Fe-SAC. Unlike most 2D graphitic supports, which usually don't disperse in solvent by themselves due to strong π…π interaction, **Fe@POG-OH** disperses in water or ethanol immediately upon sonication as shown in Fig. S15c, and the dark yellow aqueous or ethanolic dispersion can stabilize for hours without any appreciable precipitation. The good dispersion is attributed to the inherited structural features from the building units. As shown by the single-crystal structures of various hexabenzocoronene derivatives [27], these highly conjugated molecules are far from being planar, and instead they exhibit bent and curved shapes, which can frustrate dense packing and therefore is conducive to the formation of a porous and dispersible polymer. The dimethyl groups on the fluorene can provide steric bulkiness to further reduce the layer interaction in **Fe@POG-OH**. Geometry optimization of **POG-OH** performed with the Forcite module in Material Studio 6.0 (details in supporting information) reveals the overall wavy shape with these bent and bulky groups preventing the formation of a flat structure (Fig. S15a). During the preparation of our manuscript, we also noticed a very recent publication demonstrating the inherent wavy

nature of a similar COF based on hexabenzocoronene building blocks, confirming our analysis [28].

Fe-POG-OH is then examined as the catalyst for organic reactions since its pores can provide diffuse pathways for reactants to reach the active Fe centers, and therefore would expose Fe atoms in the bulk to the reactants. The dispersity can further reduce the diffusion length of the reactants for a high reaction rate. With the unique environment around the iron centers, high catalytic performance is expected.

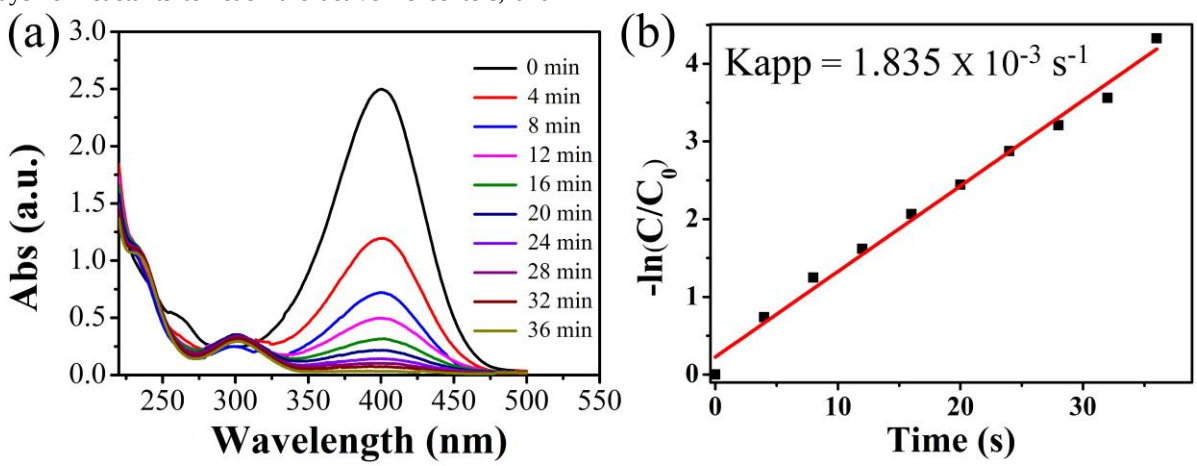

Figure 3. (a) Time-dependent UV-vis. spectra of the 4-NP reduction by $NaBH_4$ catalyzed by **Fe@POG-OH**, (**b)** Consumption rate of 4-NP: -ln (C_t /C_0) vs reaction time (bottom, R^2 = 0.98).

Fe-POG-OH is then examined as the catalyst for organic reactions since its pores can provide diffuse pathways for reactants to reach the active Fe centers, and therefore would expose Fe atoms in the bulk to the reactants. The dispersity can further reduce the diffusion length of the reactants for a high reaction rate. With the unique environment around the iron centers, high catalytic performance is expected. The reduction of nitro into amino groups is one important chemical transformation in both pharmaceutical and fine chemical synthesis.[29] In addition to hydrogen gas, sodium borohydride ($NaBH_4$) has also been used as the reductant, and its benign reducing condition is advantageous. Among many catalysts used in nitroaromatics reduction with $NaBH_4$, iron-based ones usually perform less effectively than other transition metal catalysts, such as gold [30] and Pt [31]. Although iron-based catalysts can significantly alleviate the global dependence on these expensive low-abundance elements, there is currently an urgent need to improve their catalytic performance, and we expect that **Fe@POG-OH** can greatly improve the catalytic efficiency due to single-atom distribution of Fe atoms and good dispersion.

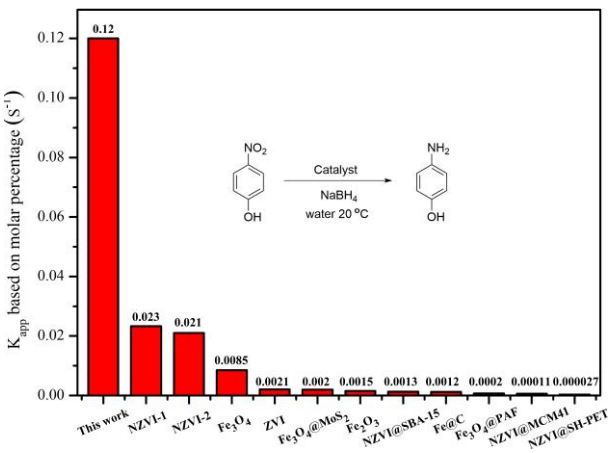

Figure 4. Comparison between K_{app} normalized with molar percentage of iron relative to the amount of p-nitrophenol. ZVI stands for zero-valent iron particles, NZVI stands for nanoscale zero-valent iron particles. Detailed analysis is available in Table S3 in the supporting information.

We examine the 4-nitrophenol (4-NP) reduction at room temperature in water with $NaBH_4$ concentration of 0.217 M and 4-NP concentration of 1.3×10^{-4} M in 2.3 ml water. As suggested by previous reports, [32] the amount of $NaBH_4$ is added in great excess to make the reaction kinetics pseudo-first-order. After mixing of 4-NP and $NaBH_4$, a solution of **Fe@POG-OH** in water (1 mg/mL, 50 μL, $4.5*10^{-6}$ mmol, 1.5 mol% relative to 4-NP (based on 1.5mol% Fe in **Fe@POG-OH**) is introduced, and then the reaction progress is monitored with the UV-vis spectroscopy. As shown in Fig. 3, it is surprising to find that at such a low loading of **Fe@POG-OH**, the K_{app} reaches as high as

1.835×10^{-3} s^{-1}, measured by the UV-vis adsorption at 400 nm of 4-NP. Considering the usage of 1.5 mol% Fe, this K_{app} translates into a normalized mole-based value of 0.123 s^{-1} (0.001835 s^{-1}/0.015). As shown in Fig. 4, **Fe@POG-OH** has highest molar K_{app} among iron-based heterogeneous catalyst. We attribute the fast kinetics of **Fe@POG-OH** to the single-atom distribution of high-spin iron atoms and excellent solution dispersion. Hot filtration experiment is performed to validate the heterogeneous nature of the reaction, with the observation that the reaction immediately stops after filtration.

Conclusion

In summary, a high-spin Fe-SAC (**Fe@POG-OH**) has been purposefully designed and synthesized under benign conditions through the utilization of strong iron/catechol interaction. **Fe@POG-OH** exhibits fast catalytic kinetics in the $NaBH_4$ reduction to 4-nitrophenol. The modular synthesis of **POG-OH** also provides opportunities for fine-tuning its reactivity in the future. Given the strong affinity of catechol with a wide of range of transition metal ions, we propose that **POG-OH** will provide a new way to prepare various transition metal SACs for heterogeneous catalysis.

Acknowledgement

This work was supported by Beihang University Research Fund 74004601, Youth 1000 Talent Fund KZ37029501, and the 111 Project (B14009).

If your manuscript has Electronic Supporting Information, a statement of the availability should be placed in this section as follows:

Supporting Information is available on

References and Notes

1 A. Wang, J. Li, T. Zhang, *Nat. Rev. Chem.* **2018**, *2*, 65-81.

2 J. Liu, M. Jiao, L. Lu, H. M. Barkholtz, Y. Li, Y. Wang, L. Jiang, Z. Wu, D.-j. Liu, L. Zhuang, C. Ma, J. Zeng, B. Zhang, D. Su, P. Song, W. Xing, W. Xu, Y. Wang, Z. Jiang, G. Sun, *Nat. Commun.* **2017**, *8*, 15938.

3 Q. Feng, S. Zhao, Y. Wang, J. Dong, W. Chen, D. He, D. Wang, J. Yang, Y. Zhu, H. Zhu, L. Gu, Z. Li, Y. Liu, R. Yu, J. Li, Y. Li, *J. Am. Chem. Soc.* **2017**, *139*, 7294-7301.

4 X. Wang, W. Chen, L. Zhang, T. Yao, W. Liu, Y. Lin, H. Ju, J. Dong, L. Zheng, W. Yan, X. Zheng, Z. Li, X. Wang, J. Yang, D. He, Y. Wang, Z. Deng, Y. Wu, Y. Li, *Journal of the American Chemical Society* **2017**, *139*, 9419-9422.

5 T. Li, F. Liu, Y. Tang, L. Li, S. Miao, Y. Su, J. Zhang, J. Huang, H. Sun, M. Haruta, *Angew. Chem. Int. Ed*. **2018**, *57*, 7795-7799.

6 Z. Zhang, J. Sun, F. Wang, L. Dai, **2018**, *57*, 9038-9043.

7 M. Zhang, Y. Wang, W. Chen, J. Dong, L. Zheng, J. Luo, J. Wan, S. Tian, W. Cheong, D. Wang, *Angew. Chem. Int. Ed*. **2017**, *139*, 10976-10979.

8 J. Gu, C. Hsu, L. Bai, H. M. Chen, X. Hu, Science. **2019**, *364*, 1091-1094.

9 D. Deng, X. Chen, L. Yu, X. Wu, Q. Liu, Y. Liu, H. Yang, H. Tian, Y. Hu, P. Du, *Sci. Adv*. **2015**, *1*.

10 Y. Xue, B. Huang, Y. Yi, Y. Guo, Z. Zuo, Y. Li, Z. Jia, H. Liu, Y. Li, *Nat. Commun.* **2018**, *9*, 1460.

11 T. R. Dugan, E. Bill, K. C. Macleod, W. W. Brennessel, P. Holland, Inorg. Chem. **2014**, *53*, 2370-2380.

12 E. R. King, E. T. Hennessy, T. A. Betley, *J. Am. Chem. Soc.* **2011**, *133*, 4917-4923.

13 P. R. Holland, *Acc. Chem. Res.* **2015**, *48*, 1696-1702.

14 E. I. Solomon, T. C. Brunold, M. I. Davis, J. N. Kemsley, S. Lee, N. Lehnert, F. Neese, A. J. Skulan, Yang, Yishan, J. Zhou, *Chem. Rev*. **2000**, *100*, 235-350.

15 W. Liu, L. Zhang, X. Liu, X. Liu, X. Yang, S. Miao, W. Wang, A. Wang, T. Zhang, *J. Am. Chem. Soc.* **2017**, *139*, 10790-10798.

16 R. K. Hocking, S. DeBeer George, K. N. Raymond, K. O. Hodgson, B. Hedman, E. I. Solomon, *J. Am. Chem. Soc.* **2010**, *132*, 4006-4015.

17 M. J. Harrington, A. Masic, N. Holten-Andersen, J. H. Waite, P. Fratzl, Science. **2010**, *328*, 216-220.

18 E. Carrington, J. Gosline, *Am. Malacol. Bull*. **2004**, *18*.

19 T. B. Karpishin, M. S. Gebhard, E. I. Solomon, K. N. Raymond, *J. Am. Chem. Soc.* **1991**, *113*, 2977-2984.

20 Q. Zhang, H. Peng, G. Zhang, Q. Lu, J. Chang, Y. Dong, X. Shi, J. Wei, *J. Am. Chem. Soc*. **2014**, *136*, 5057-5064.

21 C. J. Thambiliyagodage, S. Ulrich, P. T. Araujo, M. Bakker, *Carbon.* **2018**, *134*, 452-463.

22 D. Hulicova-Jurcakova, M. Seredych, Q. Bandosz, *Adv. Funct. Mater.* **2008**, *19*, 438-447.

23 P. Veerakumar, R. Madhu, S. M. Chen, V. Veeramani, C. T. Hung, P. H. Tang, C. B. Wang, S. Liu, *J. Mater. Chem. A.* **2014**, *2*, 16015-16022.

24 J. Jagiello, M. Jaroniec, *J. Colloid, Interf. Sci*. **2018**, *532* 588-597.

25 H. Ozawa, S. Kusaba, M. Matsunaga, M. Haga, *Langmuir.* **2018**, *34*, 2952-2958.

26 D.-H. Jo, Y.-M. Chiou, L. Que, *Inorg. Chem.* **2001**, *40*, 3181-3190.

27 J. Luo, X. Xu, R. Mao, M. Qian, *J. Am. Chem. Soc.* **2012**, *134*, 13796-13803.

28 M. Martinezabadia, C. T. Stoppiello, K. Strutynski, B. Lermaberlanga, C. Martigastaldo, A. Saeki, M. Melle-Franco, A. Khlobystov,A. Mateoalonso. J. Am. Chem. Soc. **2019**, *141*, 14403-14410.

29 M. Orlandi, D. Brenna, R. Harms, Reentje, S. Jost, M. Benaglia, *Org. Process Res. Dev*. **2018**. *22*, 430-445.

30 T.B. Nguyen, C.P. Huang, R. Dong, *Appl. Catal. B-Envion*. **2019**, *240*, 337-347.

31 S. Lu, Y. Hu, S. Wan, R. Mccaffrey, W. Zhang, **2017**, *139*, 17082-17088.

32 S. K. Ghosh, M. Mandal, S. Kundu, Nath, T. Pal, *Appl. Catal. A-Gen*. **2004**, *268*, 61-66.